Integral Solution of Equiaxed Solidification with an Interface Kinetics Model for Nuclear Waste Management

G. F. Naterer [1]

Abstract

In this paper, a one-dimensional analysis of energy and species transport during binary dendritic solidification is presented and compared to experimental results. The paper's objective is a continuation of previous studies of solidification control for the waste management of nuclear materials in the underground disposal concept. In the present analysis, interface kinetics at the solid - liquid interface accounts for recalescent thermal behaviour during solidification. The theoretical results were compared to avaliable experimental results and the agreement appears fair although some discrepancies have been attributed to uncertainties with thermophysical properties.

Nomenclature	
c	specific heat $[J/kgK]$
C	solute mean composition
D	mass diffusivity $[m^2/s]$
f	mass fraction
Fo	Fourier number $[\alpha t/X^2]$
k	conductivity or partition ratio
K	permeability $[m^2]$
L	latent heat of fusion $[J/kg]$
p	pressure $[Pa]$
Ra	Rayleigh number
T	temperature [K]
v	cartesian velocity $[m/s]$
X	reference length [m]
Greek	
α	thermal diffusivity $[m^2/s]$
β	expansion coefficient $[1/K]$
ν	kinematic viscosity $[m^2/s]$
ρ	density $[kg/m^3]$
Subscripts	
k	phase k
L, S	liquid, solid
T	temperature
C	concentration
o	reference value or initial state

Introduction

The Canadian Nuclear Fuel Waste Management Program has devoted more than a decade to the assessment and development of the underground fuel disposal concept. In this proposal, nuclear fuel waste from Canada's nuclear reactors will be deposited in a vault and excavated in plutonic rock of the Canadian Shield. A primary concern of the Environental Assessment Panel is the selection of materials and designs for the different engineering components of the disposal system [1]. Several studies have been performed on the safety and durability of the concept with the fundamental obligation to protect and avoid burdening future generations with potential environemtnal problems.

In the disposal concept, the nuclear waste container and surrounding materials provide barriers to radioactive emissions (Fig. 1). Lead - antimony metal alloys have been proposed for waste containers because of their favourable mechanical and corrosion properties. Process control of the casting solidification is essential for the prevention of container corrosion, diffusion of materials through the containers and reduction of casting defects which could provide paths for radionuclide release through the castings. In order to assist these objectives, this work continues previous studies of analytical and numerical simulation control of nuclear waste casting processes [2, 3].

In binary alloy solidification processes, two primary microstructures, i.e. columnar and equiaxed structures, form from the liquid phase [4]. In casting applications columnar structures grow out from the mould (heat sink) in an *opposite* direction to the heat flow direction whereas equiaxed grains grow in an undercooled melt region (heat sink) in the *same* direction as the heat flow direction

---

[1] Assistant Professor of Mechanical Engineering, Univeristy of New Brunswick, Fredericton, New Brunswick.

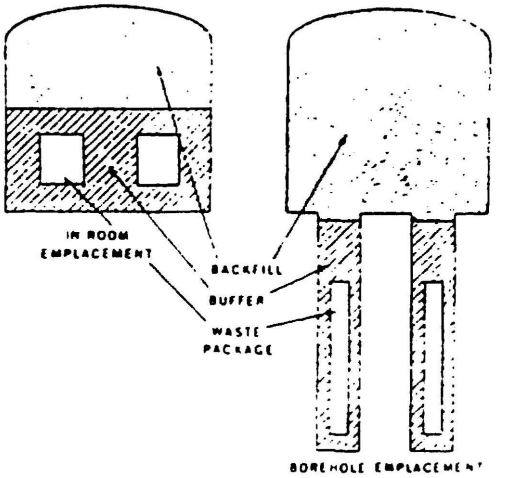

Figure 1: Nuclear Waste Disposal

Therefore, if a thermocouple was placed at a fixed location in the melt region, different cooling curves would be recorded in both cases.

In columnar growth, since heat conduction occurs through the crystals into the mould in an opposite direction to their growth, the melt region remains the hottest section of the system and the thermocouple temperature declines throughout the solidification process. In the equiaxed case, the latent heat released from the crystal must be removed from the crystal through the melt region, i.e. the melt region must be undercooled and the crystal remains the hottest section. If the latent energy release exceeds the heat extraction rate, a local heating or *recalescence* and remelting stage may occur with potentially detrimental effects on final casting properties. For example, in the presence of thermosolutal convection, remelting stages may invoke species segregation or shrinake defects in the casting.

Previous solidification studies with binary aqueous mixtures such as $NH_4Cl - H_2O$ have revealed recalescence but its prediction has been limited by an inability to precisely determine solidus and liquidus interface locations [5]. Backman and co-workers have observed thermal fluctuations which lack accountability during casting processes [6]. Predictive capabilities of this behaviour are critical factors in the final implementation of a high quality casting design for the nuclear waste containers.

In this paper, theoretical studies examine solidification of a binary $NH_4Cl - H_2O$ mixture inside a rectangular domain. The studies extend previous developments which have addressed numerical simulation issues in relation to casting processes in nuclear waste management [2, 3]. A quantitative analysis examines one-dimensional energy and species transfer at a microscopic level during the casting solidification. Comparisons between experimental and theoretical results provide a validation of the correlations between the interface kinetics and the interphase heat transfer.

Model Formulation

The general continuum equations for conservation of species, mass, momentum and energy during binary constituent phase transition may be expressed in the following form [7].

$$\frac{\partial(\rho C)}{\partial t} + \nabla\cdot(\rho\vec{v}C) = \nabla\cdot\left(\sum_1^2 \frac{f_k}{Le}\rho D_k \nabla C_k\right) + \nabla\cdot\left[\rho\vec{v}C - \sum_1^2 f_k\rho_k\vec{v}_k C_k\right] \qquad (1)$$

$$\frac{\partial\rho}{\partial t} + \nabla\cdot(\rho\vec{v}) = 0 \qquad (2)$$

$$\frac{\partial(\rho\vec{v})}{\partial t} + \nabla\cdot(\rho\vec{v}\vec{v}) = -\nabla p + (Pr)\nabla\cdot\left[\sum_{k=1}^2 \nu_k \nabla(f_k\vec{v}_k)\right] + \nabla\cdot\left[\rho\vec{v}\vec{v} - \sum_{k=1}^2 f_k\rho\vec{v}_k\vec{v}_k\right] + \beta_T(T - T_0) + \vec{G} \qquad (3)$$

$$\frac{\partial(\rho h)}{\partial t} + \nabla\cdot(\rho\vec{v}h) = \nabla\cdot(k\nabla T) + \nabla\cdot\left(\rho\vec{v}h - \sum_{k=1}^2 \rho_k\vec{v}_k h_k\right) \qquad (4)$$

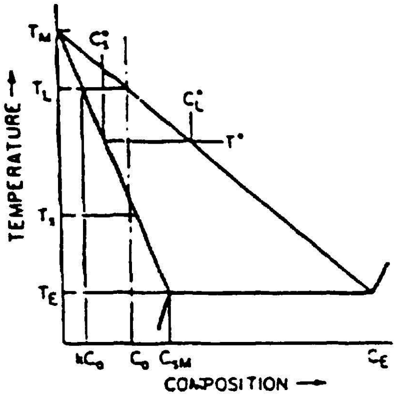

Figure 2: Binary Phase Diagram

where the phase enthalpy, h_k, was defined by

$$h_k(C,T) = \int_{T_0}^{T} c_{r,k}(\zeta)d\zeta + h_{r,k}(C,T) \quad (5)$$

In Eq. (1), $Le = \alpha/D$ denotes the Lewis number. In Eq. (3), $Pr = \nu/\alpha$ and $\vec{G}$ represent the Prandtl number and phase interaction forces, respectively. The latter term, $\vec{G}$, was determined from Darcy's Law, $\vec{G}K = \nu f_L(\vec{v}_L - \vec{v}_S)$. In Eq. (5), $c_{r,k}(T)$ refers to the reference specific heat of phase k. The governing equations must be solved with the binary phase diagram (Fig. 2) in conjunction with initial and boundary conditions for the solute composition, mixture velocity, pressure and temperature fields.

A finite element - volume scheme [7] has been employed for the solution of the continuum equations [8]. In the numerical scheme, the solid phase was presumed stationary ($\vec{v}_S$=0) and $\rho_S = \rho_L$ was assumed in order to maintain mixture saturation (i.e. the sum of phase volume fractions equals one). Thermophysical properties for the liquid, solid and mushy regions were mass-weighted by their respective mass fractions, i.e. $\alpha = f_S\alpha_S + f_L\alpha_L$. Additional details about the numerical procedure appear in Ref. [7].

Energy and Species Transport Models

In the following diffusion-dominated analysis, consider a one-dimensional volume which moves at a velocity $V(t)$ with the phase interface,

$$\frac{\partial C}{\partial t} = D\frac{\partial^2 C}{\partial x^2} \quad (6)$$

$$\rho c_P \frac{\partial T}{\partial t} = k\frac{\partial^2 T}{\partial x^2} + \rho L\frac{\partial f_S}{\partial t} \quad (7)$$

subject to

$$C_L(t=0) = C_0 \qquad T(t=0) = T_0 \quad (8)$$

$$-D\left.\frac{\partial C}{\partial x}\right|_R = C_L(1-k_P)V; \quad C_L|_\infty = C_0 \quad (9)$$

$$-k\left.\frac{\partial T}{\partial x}\right|_L + k\left.\frac{\partial T}{\partial x}\right|_S = \rho VL; \quad T|_\infty = T_0 \quad (10)$$

where $R(t)$ is the interface position and the subscript ∞ refers to a far-field condition.

Integrating Eq. (6) from $x = R - \infty$,

$$\frac{\partial}{\partial t}\int_R^\infty C_L(x,t)dx = C_L(1-k_P)V(t) \quad (11)$$

Assuming an exponential concentration profile within the liquid phase [9],

$$C_L = \frac{C_0}{k_P}exp[-V(t)(x - R(t))/D] \quad (12)$$

Substitution of Eq. (12) into Eq. (11) and simplification yields a 1st-order differential equation for $V(t)$,

$$\frac{dV}{dt} + \left(\frac{1-k_P}{D}\right)V^3 = 0 \quad (13)$$

Solving Eq. (13) subject to $V(t=0) = V_i$,

$$V(t) = V_i\sqrt{\frac{1}{1+\kappa t}} \qquad \kappa = \frac{2(1-k_P)}{D}V_i^2 \quad (14)$$

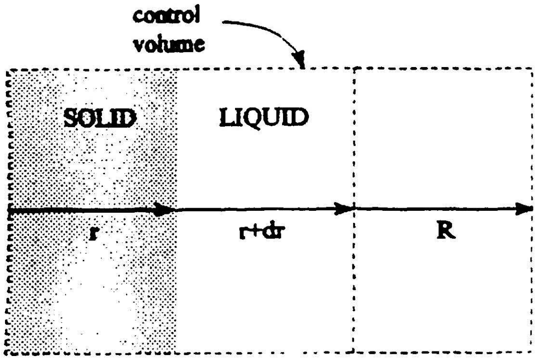

Figure 3: One-Dimensional Crystal Growth

In physical terms, as the solution approaches a steady-state ($t \rightarrow \infty$), conduction into the interface balances the latent heat release from the interface and the interface becomes stationary, i.e. $V(t) \rightarrow 0$ in Eq. (14).

Considering one-dimensional planar crystal growth in the radial direction, r (see Fig. 3), $df_S/dt \approx V(t)/R$ for crystal growth from a nucleation site ($t = 0$) in an isothermal ($T = T_0$) and undercooled liquid region,

$$\frac{\partial^2 T}{\partial x^2} = 0; \quad \frac{f_S}{\partial t} > 0 \tag{15}$$

Thus, from Eq. (7), $\frac{\partial T}{\partial t} > 0$ (recalescence occurs) and the temperature increases from $T_0(t = t_0)$ to some $T(t = t_1) = T_1$ over a time interval $\Delta t > 0$. Assuming heat transfer from the volume occurs at a uniform rate, $\alpha \nabla^2 T \approx -q[K/s]$, then the recalescence period occurs until $(\frac{\partial T}{\partial t})_{t_1} = 0$, i.e. from Eq. 14),

$$\frac{\partial T}{\partial t} = -q + \frac{L}{c_P}\left[\frac{V_i}{R}\sqrt{\frac{1}{1+\kappa t}}\right] = 0 \tag{16}$$

where $\Delta t = t_1 - t_0$ and $q > 0$. Equation (16) may be written as

$$\Delta t = \frac{D}{2(1-k_P)}\left[\left(\frac{L}{qc_P R}\right)^2 - \left(\frac{1}{V_i}\right)^2\right] \tag{17}$$

The initial crystal growth rate, V_i, varies in an exponential manner as a function of the interface Gibbs energy, ΔG [4],

$$V_i = V_0 exp\left(-\frac{\Delta G}{k_B T}\right) \tag{18}$$

where $k_B = 1.38 * 10^{-23}[J/K]$ is the Boltzmann constant and ΔG represents the energy required to maintain crystal bonds in the lattice structure from melting back to the liquid. The Gibbs energy may be written in terms of the interface energy, $\sigma[J/m^2]$, and the entropy of fusion per unit volume, $\Delta s[J/m^3 K]$ [4],

$$\Delta G \approx \frac{16\pi}{3}\frac{\sigma^3}{\Delta s^2 \Delta T^2} \tag{19}$$

where ΔT is the undercooling level prior to the onset of solidification.

Substituting Eqs. (18) and (19) into Eq. (17),

$$\Delta t \approx \left[\frac{D}{2(1-k_P)}\left(\left(\frac{L}{qc_P R}\right)^2 - \left(\frac{1}{V_0}\right)^2\right) - \right] - \left[\frac{D}{2(1-k_P)}\frac{32\pi\sigma^3}{3k_B \Delta s^2 T V_0^2}\right] / \Delta T^2 \tag{20}$$

or $\Delta t \approx A - B/\Delta T^2$. This equation intersects the ΔT axis at $\Delta T_0 = \sqrt{B/A}$ where recalescence will not be observed for $\Delta T \leq \Delta T_0$. Equation (20) demonstrates the recalescence period increases with the undercooling level, ΔT; in words, the crystal growth rates increase exponentially with ΔT and this rapid growth leads to a rapid latent heat release within the crystal which exceeds its heat transfer rate out across the volume edges.

In the present experiments, $\sigma \approx \Gamma \Delta s = 10^{-4}[J/m^2]$ from the definition of the Gibbs -

Thompson coefficient, Γ. Also, $q \approx 0.025[K/s]$ and $R \approx 4[mm]$ from the experiments and $V_0 \approx 0.01[mm/s]$ from crystal growth measurements in Ref. [10]. Thus, Eq. (20) may be written as

$$\Delta t[min] \approx 0.277 - 17.73/\Delta T^2 \qquad (21)$$

where property values for the $NH_4Cl - H_2O$ solution have been employed.

Experimental Procedures

Experiments were conducted with an aqueous ammonium chloride solution ($NH_4Cl - H_2O$) inside a rectangular enclosure. The experiments consisted of photographic observations of the phase interface motion and thermocouple measurement of the internal temperature distribution during solidification. In addition, discrete particles within the mixture were employed for the observation of fluid streak lines. Identical experiments were conducted twice to establish repeatable results.

A thermocouple grid was construcuted and placed inside the enclosure to monitor the transient temperature profiles in each test. The grid consisted of 16 $Co - Cu$ 0.5$[mm]$ diameter bare wire thermocouples which were soldered at the midplane within a plexiglass frame citeaiaa29. Constantan - Copper (Type T) thermocouples were employed. The thermocouple frame was inserted into the test cell before each simulation. The horizontal locations of each thermocouple column within the grid were 0.64$[cm]$, 2.54$[cm]$, 5.72$[cm]$ and 7.62$[cm]$, respectively. The vertical locations of each thermocouple row within the grid were 0.64$[cm]$, 2.54$[cm]$, 5.08$[cm]$ and 7.62$[cm]$, respectively. The thermocouples were numbered from 1 to 4 (column 1; top to bottom), 5 to 8 (column 2; top to bottom), 9 to 12 (column 3; bottom to top) and 13 to 16 (column 4; bottom to top).

In each experiment, the side and base walls were maintained at sub-zero conditions and the top surface was a free boundary exposed to a quiescent air layer under the thermocouple frame. These conditions generated columnar dendritic growth along the walls as well as thermal and solutal convection patterns with crystal sedimentation inside the cavity (Figs. 1b and 1c). Further details of the experimental diagnostics and setup conditions appear in Ref. [11].

Results and Discussion

(I) Case 1 ($T_0 = 318[K], C_0(H_2O) = 0.72$)

In the early stages of solidification, the liquidus interface developed nearly uniformly across each cell wall. At subsequent stages, thermal and solutal buoyancy in the liquid regions generated a convection cell on each side of the cavity. The interaction between the upward convection transport of crystals from the lower mushy region and each crystal's weight created a downward sedimentation process along the cell vertical midplane [11]. At the steady-state ($t \approx 6880[s]$), the multiphase region profile illustrates the approximate problem symmetry about the vertical midplane (Fig. 4).

Interior temperatures in Figs. 5-6 decline in a monotonic manner except locations 6 - 8 where local heating or *recalescence* creates a temporary thermal fluctuation at $t \approx 370[s]$. These results appear consistent with recalescence observations of other researchers, i.e. Refs. [5, 10]. A period of recalescence, $\Delta t > 0$, occurs when the latent heat release within a crystal exceeds conduction of sensible heat from the solid - liquid region around the crystal thereby creating a local heating effect. This rate of latent heat release increases with the

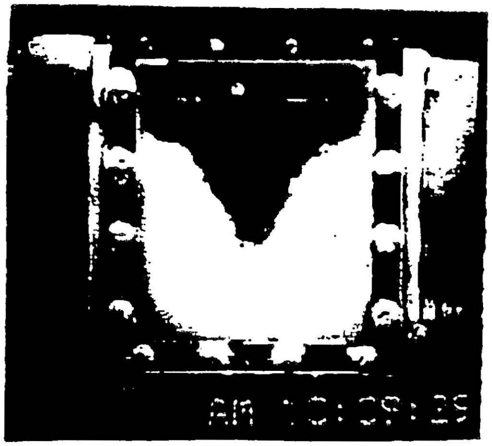

Figure 4: Case 1. Solidification Results

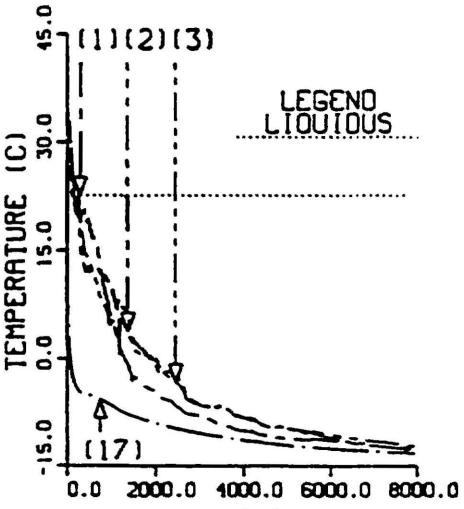

Figure 5: Case 1. Thermocouple Results

undercooling level, $\Delta T = T_{LIQ} - T$, because fewer atoms have sufficient energy to melt back into the liquid near the phase interface at high undercooling levels. Therefore, recalescence occurs primarily at high undercooling levels.

The previous unidirectional heat and species transfer analysis has shown that the recalescence period varies as $\Delta t[min] \approx 0.277 - 17.73/\Delta T^2$. Only points beyond the intersection between the $\Delta t - \Delta T$ curve and the ΔT axis demonstrate recalescence because the solid growth exceeds the heat transfer from the interface in this region. Experimental results in Case 2 will further examine these trends between recalescence and undercooling levels.

Additional observations were directed towards qualitative aspects of the crystal sedimentation process along the cell midplane. These aspects pertain to (i) thermal conditions which affect the crystal's maximum height prior to its reversal and sedimentation and (ii) whether a minimum crystal size exists below which a crystal will not settle.

Firstly, after a crystal's weight exceeded its upward acceleration along the cell midplane, it decelerated and eventually descended and created an inverted V-shaped sedimentation layer along the lower boundary (Fig. 4). Since the crystal sizes and weights were different, their descents initiated at different heights. In fact, the thermal conditions affect the crystal's maximum height prior to its reversal and sedimentation. For example, consider a crystal's ascent from a lower section 8 with a fixed pressure gradient and initial velocity at location 8 but variable thermal conditions which generate different crystal trajectories. Cases with a lower thermal gradient in the positive y-direction will initiate a shorter crystal trajectory. From Figs. 5-6, we observe the rate of temperature decline at location 8 exceeds the decline rate at location 6 during the period of sedimentation.

Secondly, the NH_4Cl-rich crystals have a higher density than the liquid phase. Thus, the crystals settle downwards along the cell midplane unless they remelt before their flow reversal downwards. If a crystal reverses its ascent, it accretes and grows during its descent which prevents any subsequent flow re-

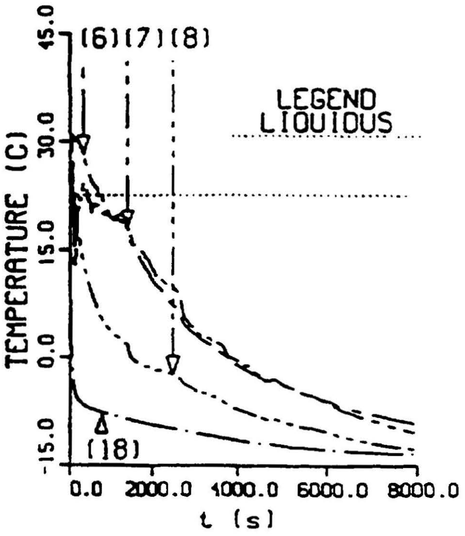

Figure 6: Case 1. Thermocouple Results

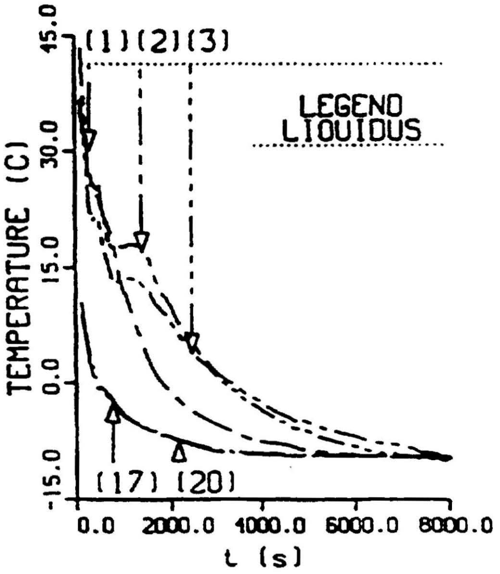

Figure 7: Case 2. Thermocouple Results

versal. Qualitative observations confirmed no crystals ascended after their formation or reversed their decent. An exception occurred along the side boundaries near the liquidus interface where brief crystal upflows were observed. Solutal buoyancy as a result of solute enrichment of lighter solute (H_2O) near the interface may have been a factor which initiated these temporary upflows.

(II) Case 2 ($T_0 = 318[K], C_0(H_2O) = 0.68$)

In this case, crystal sedimentation in the form of an inverted V-shaped layer was not observed because the columnar growth developed faster in this case in comparison to the previous case (i.e. a larger initial undercooling level of the wall temperature below the liquidus temperature due to $C_0(case\ 2) < C_0(case\ 1)$). Since columnar grains developed rapidly in comparison to Case 1, the convection cells had less strength to detach crystals from the mushy region.

Thermocouple measurements appear in Figs. 7-8; a similar pattern of warmer temperatures near the stagnation point arises at location 6. Also, Fig. 8 illustrates the higher undercooling level in this case prolongs the recalescence period at $t \approx 370[s]$ in comparison to the previous case. In fact, a larger early recalescence period preceeds subsequent short recalescence periods at locations 6 - 8. Recalescence promotes repetitive thermal behaviour. For example, if a crystal reheats a solid - liquid mixture, it may melt the solid region back to the liquid phase; subsequent solute transfer would undercool the region and once again generate thermal recalescence albeit with a lower magnitude. Heat transfer from the system throughout the process reduces the undercooling levels at each subsequent recalescence period.

Comparisons between experiments and theory for the duration of the first recalescence period at $t \approx 370[s]$ in terms of the undercooling level, ΔT, appear in Fig. 9. Each set of markers for locations 6 and 7 represent different experiments (cases (i) - (iii)) at $t \approx 370[s]$ (onset of recalescence). The recalescence period, Δt, was defined as the duration

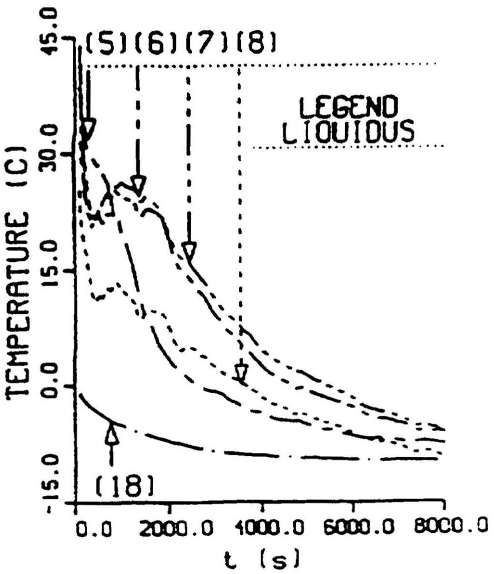

Figure 8: Case 2. Thermocouple Results

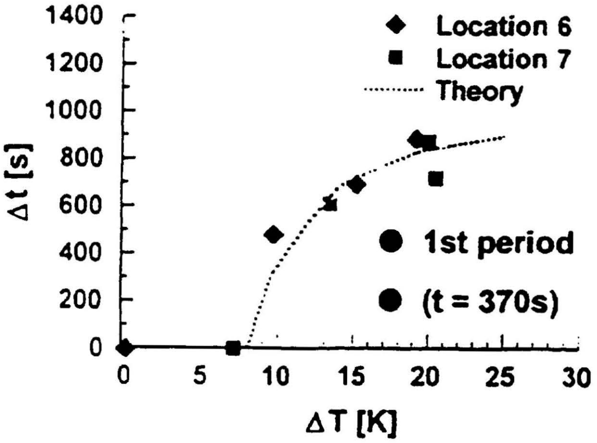

Figure 9: Recalescence Results

between $t \approx 370[s]$ and the time where the temperature declined below a local maximum by $0.5[K]$. The undercooling level, ΔT, was defined as the temperature difference between the thermocouple measurement at $t \approx 370[s]$ and $T_{LIQ}(C_0)$. Fair agreement was achieved between the theoretical model, $\Delta t[min] \approx 0.277 - 17.73/\Delta T^2$, and the experimental results. The results demonstrate how recalescence arises from undercooled conditions; high undercooling levels (i.e. $\Delta T \approx 21[K]$) promote rapid nucleation and long recalescence periods whereas low undercooling levels (i.e. $\Delta T < 8[K]$) initiate nucleation at a rate which releases latent heat slower than conduction of sensible heat from the crystal (i.e. no recalescence).

Conclusions

Experiments and an analysis of solidification of a binary $NH_4Cl - H_2O$ mixture were conducted in a rectangular domain. Measurements were performed with thermocouples, photographic techniques and digital image analysis. The duration and magnitude of recalescence was augmented at larger liquid undercooling levels and an integral solution technique supported these observations. Free crystal convection diminished with lower thermal gradients in the y-direction. Also, crystal sedimentation paths were broadened over the duration of their descent. These theoretical and experimental developments will serve in future models of casting processes in nuclear waste management.

References

1. Allan, C., "Nuclear Fuel Waste Disposal - AECL's Concept and the Importance of Implementation", *Canadian Nuclear Society Bulletin*, vol.14, no.1, pp.19-23, 1993.

2. Naterer, G. F., Schneider, G. E., "Species Redistribution During Solidification of Nuclear Fuel Waste Metal Castings", Proceedings, CNA/CNS 18th Nuclear Sci-

ences Student Conference, Montreal, 1993.

3. Naterer, G. F., Schenider, G. E., "Anisotropic Permeability model of Casting Processes for Nuclear Waste Management", Proceedings, CNA/CNS 19th Nuclear Sciences Student Conference, Toronto, 1994.
4. Kurz, W., Fisher, D. J., *Fundamentals of Solidification*, Trans Tech Publications, Switzerland, 1989.
5. Cristenson, M. S., Bennon, W. D., Incropera, F. P., *International Journal of Heat and Mass Transfer*, vol.32, no.1, pp.69-79, 1989.
6. Backman, D. G., Mehrabian, R., Flemings, M. C., *Metallurgical Transactions*, vol.8b, pp.471-477, 1977.
7. Naterer, G. F., Schneider, G. E., "PHASES Model of Binary Constituent Solid - Liquid Phase Transition - Part 1. Numerical Method", *Numerical Heat Transfer B*, vol.8, no.2, pp.111-126, 1995.
8. Naterer, G. F., Schneider, G. E., "PHASES Model of Binary Constituent Solid - Liquid Phase Transition - Part 2. Applications", *Numerical Heat Transfer B*, vol.8, no.2, pp.127-137, 1995.
9. Charach, C., Keizman, Y., *Computational Modelling of Free and Moving Boundary Problems*, vol.3, pp.157-164, 1995.
10. Johnston, M. H., Griner, C. S., Parr, R. A., Robertson, S. J., *Journal of Crystal Growth*, vol. 50, pp.831-838, 1980.
11. Naterer, G. F., Schneider, G. E., "Experimental Study of Dynamic and Thermal Conditions During Binary Dendritic Solidification", AIAA 29th Thermophysics Conference, San Diego, California, USA, June 19-22, 1995.